



Carotid Pressure Wave Separation Analysis Using Multi-Rayleigh Flow Model

Rahul Manoj , Member, IEEE, V. Raj Kiran , Member, IEEE, P. M. Nabeel , Member, IEEE, Mohanasankar Sivaprakasam , Member, IEEE, and Jayaraj Joseph , Member, IEEE

Abstract—Background: Wave separation analysis (WSA) performed at the common carotid artery (CCA) reveals insights into cerebral vascular pathophysiology; however, the conventional WSA (WSA_{REF}) necessitates the availability of both pressure and flow waveforms measured from the same arterial site. **Objective:** We propose a method for performing WSA at CCA using a single pulse waveform (WSA_{m-RAY}), by modelling the shape of the CCA flow using multi-Rayleigh curves. The WSA_{m-RAY} reduces the measurement complexity, by modelling the flow waveform shape, targeted at scenarios with limited resources, where comprehensive equipment, specialized personnel and hospital settings are often lacking. The modelled flow was compared with the measured flow for accuracy in modelling the flow morphology. The performance of WSA_{m-RAY} was evaluated by comparing the reflection quantification indices derived from WSA_{REF} and WSA_{m-RAY} . **Methods:** WSA_{m-RAY} employs weighted and shifted multi-Rayleigh functions, time-optimized for characteristic flow peaks in the early and late systolic phase of the CCA flow waveform. The reliability of the modelled flow and performance of WSA_{m-RAY} were validated on 70 (28 female) participants (age: 20 to 51 years). Continuous recording of CCA flow velocity and diameter waveforms were recorded from the participants. **Results:** The root-mean-squared-error in forward and backward pressure waves was 2.18 ± 0.97 mmHg ($\sim 2.5\%$ of the average mean arterial pressure of the study participants). A statistically significant and strong correlation ($r > 0.76$, $p < 0.001$) was observed among reflection quantification indices from WSA_{REF} and WSA_{m-RAY} . **Conclusion:** WSA_{m-RAY} potentially expands the scope of

vascular screenings using a single pulse measurement targeting resource constrained settings.

Index Terms—Arterial pressure, blood flow, carotid, reflection magnitude, wave separation analysis.

I. INTRODUCTION

THE common carotid artery (CCA) is one the widely preferred sites for recording non-invasive pulse waves due to its easily accessible location, proximity to the aorta, and superficial nature. These advantages make it a convenient site for non-invasive measurement of large artery stiffness and central blood pressure (BP) [1]. The carotid pressure has been used as a surrogate for ascending aortic pressure for studies related to vascular ageing, pregnancy-associated hypertension [2], and therapeutic goals for anti-hypertension treatments [3].

At any arterial site, the measured pulse waves comprise forward-traveling waves and their reflections (and re-reflections). The pulse wave reflection is a natural phenomenon resulting from the mismatch in impedances encountered by the forward-traveling wave due to the inherent heterogeneity of the vasculature [4]. However, increased or abnormal wave reflections are observed to be associated with the pathophysiology of increased systolic BP and altered ventricular dynamics, which results in increased cardiac afterload [5] and end-organ damage [6].

Separation of forward and reflected waves is essential to quantify the pulse wave reflection and is accomplished by techniques such as wave separation analysis (WSA) [7] and wave intensity analysis (WIA) [8]. Both of which requires pressure along with flow waveform measured from the aorta. However, the simultaneous measurement of pressure along with the flow is practically challenging, which requires special arrangements on ultrasound or Magnetic Resonance Imaging systems with integrated pressure sensors. The WSA can also be evaluated directly from diameter waveform [9], [10], [11], without additional conversion to pressure waveform, thus eliminating uncertainty due to the pressure calibration. Nevertheless, both the approach requires additional flow measured from the same arterial site to perform WSA, which limits the applicability of WSA only to hospital settings. Subsequently, independent researchers introduced pressure-only WSA or WSA using single pulse waveform. These approaches use carotid pressure waves obtained through tonometry-calibrated or diameter-calibrated pulse waveforms or modelled pressure waves through generalized transfer functions

Received 21 June 2024; revised 29 October 2024; accepted 27 November 2024. Date of publication 11 December 2024; date of current version 23 April 2025. This work was supported in part by the Science and Engineering Research Board (SERB), Department of Science and Technology (DST), in part by the Indian Institute of Technology (IIT) Madras under Institute of Eminence (IoE), and in part by the Ministry of Human Resource Development (MHRD), Government of India. (Corresponding author: Rahul Manoj.)

Rahul Manoj is with the Department of Electrical Engineering, Indian Institute of Technology Madras (IIT M), Chennai 600036, India (e-mail: rahulmanojkty@gmail.com).

V. Raj Kiran is with the Department of Electrical Engineering, Indian Institute of Technology Madras (IIT M), India.

P. M. Nabeel is with the Department of Electrical Engineering, Indian Institute of Technology Madras (IIT M) and Healthcare Technology Innovation Centre (HTIC), IIT M Research Park, India.

Mohanasankar Sivaprakasam is with the Faculty of Electrical Engineering at Indian Institute of Technology Madras (IIT M) and Healthcare Technology Innovation Centre (HTIC), IIT M Research Park, India.

Jayaraj Joseph is with the Faculty of Electrical Engineering at Indian Institute of Technology Madras (IIT M), India.

This article has supplementary downloadable material available at <https://doi.org/10.1109/TBME.2024.3515819>, provided by the authors.

Digital Object Identifier 10.1109/TBME.2024.3515819

as substitutes for aortic pressure. Additionally, they assume a flow shape model for aortic flow [12], [13], [14], [15], [16], [17] to implement aortic WSA. These approaches are proven to reduce the measurement complexity without compromising the clinical utility of WSA.

In contrast to aortic WSA, recent cross-sectional and prospective studies [18], [19], [20], [21], [22] suggest a potential link between upper body arterial phenotype and cerebral microvascular diseases leading to Alzheimer's disease, vascular dementia, and normal pressure hydrocephalus [23]. The underlying vascular pathophysiology behind these conditions is related to the strength of the pulse waves induced in the craniospinal cavity by the upper body vasculature [23]. Notably, the upper body flow waveforms are inherently different from those observed in ascending aorta or lower body arteries. The CCA flow waveform is triphasic, with distinguishable peaks in early, late systolic, and diastolic phases, which are absent in the aortic flow [22]. Recent studies that perform WSA on carotid pressure and flow waveforms were able to anticipate the onset of mild cognitive impairment over a decade before clinical diagnosis [24]. Similarly, age-related changes in carotid artery flow waveforms were quantified and were observed to have possible implications with cerebral microvascular diseases [21], [22].

In addition to carotid WSA, the WIA on carotid pressure and flow waveforms has paved the way for various physiologic perturbation studies in healthy and diseased populations relating to cardiac and cerebral hemodynamics [10], [11], [25]. The WIA applied to the carotid artery has identified intensity peaks associated with the pathophysiology of the cerebral vasculature and depicts peaks in the mid-systolic phase that are generally absent in the WIA obtained from ascending aorta [26]. Consequently, assessing carotid wave reflections would potentially provide clinical usefulness to the changes in cerebral vasculature and ventriculoarterial interaction. However, due to the tri-phasic nature of the CCA flow waveform, which is inherently different from the aorta, a direct adaptation of existing pressure-only WSA methods [12], [13], [14], [15], [16], [17], which assume an ideal aortic flow waveform, is hindered. Therefore, there is a need for modelling the CCA artery flow waveform physiologically as close to the measured flow, such that it reduces the measurement complexity for applying WSA at CCA.

In this work, we propose a simplified pressure-only WSA for CCA. The method involves modelling the shape of CCA flow waveform using weighted and shifted multi-Rayleigh functions that mimic the characteristic peaks of CCA flow. The required characteristics of the CCA flow shape are identified using pulse wave analysis of the CCA pressure waveform. The WSA using the multi-Rayleigh flow model (WSA_{m-RAY}) is implemented using the measured/derived pressure waveform and modelled flow shape to quantify the magnitude of wave reflection and its arrival time. The validation strategy involves comparing the modelled flow with the measured flow for its accuracy and correspondence of the flow shape in both time domain and frequency domain matrices and evaluating the performance of the WSA_{m-RAY} by comparing the reflection quantification indices with those from conventional WSA (WSA_{REF} , which uses measured flow). An in-vivo study was conducted on 70 healthy human participants

aged 20–51 years to validate the study objectives. The following section of the manuscript describes the construction of the flow morphology and the theory of WSA_{m-RAY} , followed by the study design, data collection and statistical analysis. The subsequent sections discuss the major observations, limitations, and future research directions.

II. MATERIALS AND METHODS

A. Construction of Multi-Rayleigh Flow Shape Approximation for CCA Flow

The triphasic CCA flow includes the early systolic flow peak, late systolic flow peak and diastolic flow peak, with a non-zero end-diastolic flow rate. However, for WSA, the systolic phase of the flow, with its pulsatile amplitude, is more relevant than the diastolic phase and the end-diastolic flow. Therefore, the modelling of flow shape using the multi-Rayleigh functions is limited only to the systolic phase of the pulse waveform. An illustration of the features of the CCA flow waveform is depicted in the supplementary Fig. 1.

The Rayleigh functions are a skewed form of Gaussian functions, with only one model parameter (σ). The Rayleigh functions offer the flexibility to modulate the steepness of its upslope and downslope using a single parameter, as opposed to multiple parameters while using Gaussians [27] and Log-normal [15]. The Rayleigh functions also offer a smoother morphology than triangular approximations [12]. The construction of the flow model assumes that any effect of pulse wave reflection on the flow morphology, would manifest in the pressure, due to their close coupling, therefore, derived features from pressure waveform – healthy or disease are used to construct the flow shape model. The steep upslope and gradual downslope of a Rayleigh function have similarities with the morphology of CCA flow waveforms. This feature of Rayleigh functions was explored as a basis for modelling flow waveforms. Fig. 1 describes the construction of the multi-Rayleigh flow waveform using pulse waveform analysis of the pressure waveform. The pressure waveform can be obtained non-invasively as a tonometry pulse waveform linearly calibrated with brachial BP or a diameter waveform non-linearly scaled to pressure and calibrated with brachial BP.

The shape of the flow waveform is modelled as a sum of weighted and shifted Rayleigh functions for the early systolic phase and late systolic phase as described in (1) and (2).

$$Q_{m-RAY}(t)|_{ES} = \sum_{i=1}^M \frac{t}{\sigma_i^2} e^{(-t^2/2\sigma_i^2)}; 0 \leq t \leq t_{SBP} \quad (1)$$

$$Q_{m-RAY}(t)|_{LS} = \sum_{j=1}^N \frac{t}{\sigma_j^2} e^{(-t^2/2\sigma_j^2)}; t_{SBP} \leq t \leq t_{ED} \quad (2)$$

Where, $Q_{m-RAY}(t)|_{ES}$ is the modelled flow waveform shape for the early systolic phase and $Q_{m-RAY}(t)|_{LS}$ is the modelled flow waveform shape for the late systolic phase, σ_i , σ_j are the model design parameters obtained by optimization of objective functions F_1 and F_2 as described in (3) and (4). The t_{SBP} is the time instant at which the pressure reaches systolic blood pressure

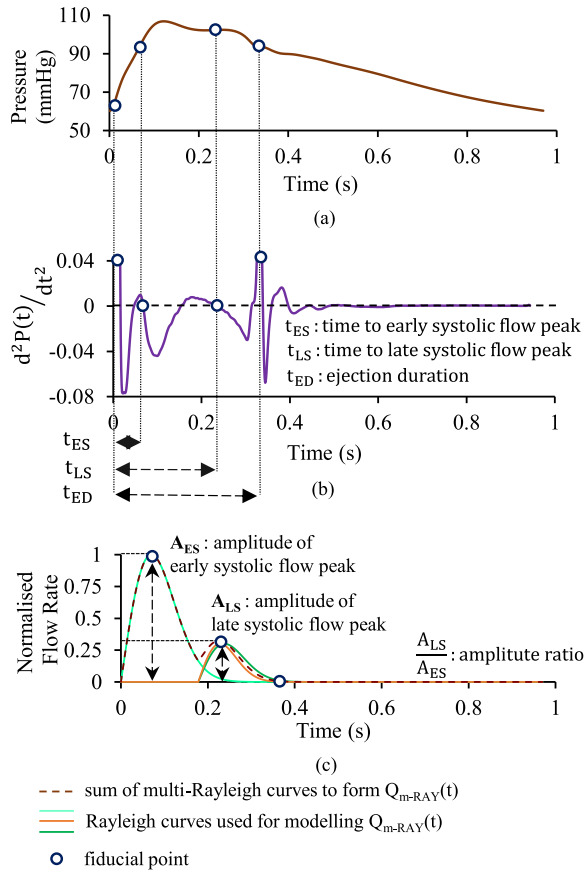


Fig. 1. Construction of multi-Rayleigh flow model $Q_{m-RAY}(t)$ (a) carotid pressure waveform $P(t)$, with its fiducial points identified, from which modelled flow shape waveform is constructed, (b) second derivative of pressure waveform used for the pulse wave analysis to identify the fiducial points (c) modelled multi-Rayleigh flow waveform.

(SBP), and t_{ED} is the ejection duration of the pulse wave. The ejection duration is the time taken from the opening of the aortic valve to the closing of the valve. M and N are the maximum number of Rayleigh functions used for optimization.

The objective functions F_1 and F_2 obtain the model design parameters (σ_i , σ_j), such that it minimizes the error between the estimated and modelled time instants of the early and late systolic peaks of the CCA flow waveform. The estimated time instants (t_{ES}) and (t_{LS}) are obtained from the zero-crossings of the 2nd derivative of pressure waveform, as illustrated in Fig. 1.

$$F_1 = \min ||T(Q_{m-RAY}(t)|_{ES \text{ Peak}}) - t_{ES}|| \quad (3)$$

$$F_2 = \min ||T(Q_{m-RAY}(t)|_{LS \text{ Peak}}) - t_{LS}|| \quad (4)$$

where, $T(Q_{m-RAY}(t)|_{ES \text{ Peak}})$ is the time instant of the early systolic flow peak and $T(Q_{m-RAY}(t)|_{LS \text{ Peak}})$ is the time instant of the late systolic flow peak from the modelled flow. The error threshold for F_1 and F_2 to converge the optimization is rationally set to 2 ms ($\sim 0.25\%$ of the average heart rate of the study population) or reaching the maximum number of Rayleigh functions to be used as in M and N of (1) and (2). They are set to a limit of 5, as in most cases, the convergence was obtained well within the maximum range. The amplitude ratio (A_{LS}/A_{ES}) of

modelled flow is obtained from the statistical regression model, derived from its association with the augmentation index of pressure waveform [22]. The details of the statistical model are described in the supplementary section. The augmentation index is computed using pulse wave analysis from the higher derivative waveforms of the pressure waveform [28]. The amplitude of the modelled flow shape is normalized to 1 A.U. (Arbitrary Unit), as illustrated in Fig. 1. However, for the computation of characteristic impedance, the amplitude of modelled flow is scaled to measured peak flow magnitude. This scaling to measured flow peak serves only for graphical illustration purpose and in no means a necessary step for WSA.

B. Wave Separation Analysis

The WSA combines the pressure-flow relationship from water hammer theory with transmission line circuit analogy to obtain expressions for forward and backward pressure waveforms as in (5) and (6) [7].

$$P_F(t) = \frac{1}{2} (P(t) + Z_C \times Q(t)) \quad (5)$$

$$P_B(t) = \frac{1}{2} (P(t) - Z_C \times Q(t)) \quad (6)$$

where, $P_F(t)$ and $P_B(t)$ are the forward and backward pressure waveform, respectively, and $Q(t)$ is the flow waveform, measured or modelled. $P(t)$ is the measured or calibrated pressure waveform. The Z_C is the characteristic impedance of the arterial segment from which $P(t)$ and $Q(t)$ are obtained. For WSA, based on the (5) and (6), the product $Z_C \times Q(t)$ becomes ratio metric, i.e., Z_C assumes an arbitrary unit, for a normalized $Q(t)$, however the product $Z_C \times Q(t)$ gets preserved. This enables to model the shape of the flow waveform and use it as a substitute of measured flow to perform WSA.

The reflection quantification indices calculated from $P_F(t)$ and $P_B(t)$ includes – pulse pressure of forward and backward wave in mmHg (ΔP_F , ΔP_B), mean values (mean P_F , mean P_B) their ratio (mean P_B /mean P_F) as %, Reflection Magnitude (RM) as a ratio of ΔP_B to ΔP_F , Reflection Index (RI) as a ratio of ΔP_B to sum of ΔP_F and ΔP_B , as %, and Reflection Wave Transit Time (RWTT), as the temporal difference between forward and backward wave, defined as in [30].

C. Instruments Used for Data Collection

Any pulse waveform recording modality – diameter from ultrasound scans, tonometry, photoplethysmogram can be used to obtain the required arterial pulse waveform from CCA. In this study, the pressure waveform required for performing the WSA and for deriving the modelled flow was obtained non-invasively from the CCA diameter waveform, which is scaled non-linearly and calibrated with mean arterial pressure (MAP) and diastolic blood pressure (DBP) obtained from brachial artery [33]. The required diameter waveforms from CCA were recorded using an in-house developed ARTSENS device [31]. The ARTSENS consists of a custom-made focused ultrasound transducer probe (center frequency: 5 MHz, diameter: 5 mm, spatial angle $< 1.3^\circ$), acquisition hardware and recording software. Details on the

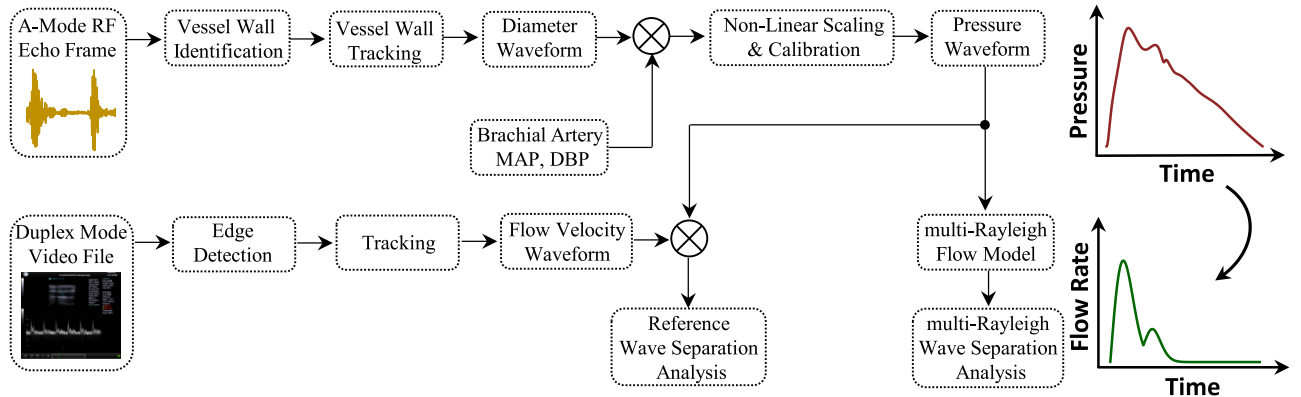


Fig. 2. Software architecture illustrating the major algorithms and signal processing steps involved as part of the data processing and analysis. .

hardware and software architecture of ARTSENS are referred elsewhere [31] and to Supplementary Section. The recorded ultrasound A-mode echo signals from the vessel walls of the left CCA were identified and tracked frame-to-frame using previously validated algorithms [32] to derive continuous diameter waveforms (frame rate: 500 Hz, tracking resolution: 10 μ m).

The measured flow required to implement the WSA_{REF} was obtained from Doppler ultrasonography-based blood flow velocity waveforms recorded using a clinical-grade ultrasound imaging system (Sonix Touch+, BK Medical). The imaging system consists of a linear array probe (center frequency: 10 MHz, pitch: 0.3 mm, depth: 4 cm). The duplex mode (frame rate: 60 Hz) with pulsed wave Doppler was utilized to record continuous flow velocity waveforms as a video file. The required measured flow is obtained by combining the diameter waveform information obtained from ARTSENS with flow velocity obtained from the Doppler sonography.

D. Study Design and Protocol

A cross-sectional study was conducted on 70 healthy human participants (28 females) aged from 20 years to 51 years. The study protocol was approved by the institute ethics committee of the Indian Institute of Technology Madras, Chennai, India (IEC/2021-01/JJ/07). The participants were informed of the study objectives. A written consent form was collected from the participants on their voluntary participation. The study protocol and data collection adhere to the latest principles and guidelines of the Declaration of Helsinki for medical research involving human subjects, as revised in 2013.

The study was conducted in a temperature-regulated room ($\sim 25^\circ\text{C}$), where the participants were asked to lie supine for twenty minutes. After five minutes of the rest phase in the supine posture, brachial cuffs were wound on the left arm, followed by brachial BP measurement using an oscillometry device (Model:247, SunTech Medical, USA). The brachial BP measurements were recorded three times, and an average BP was used for further analysis. For the CCA flow velocity measurements, the linear array probe of the ultrasound imaging system was positioned and oriented on the neck region of the

participants to obtain a clear image of the CCA in the longitudinal section. Appropriate gate width ($\sim 1/3$ rd of the lumen diameter) was configured to measure the Doppler flow velocity of the blood flow. The Duplex mode of the imaging system records the flow velocity waveforms for thirty seconds as a video file.

For measurements using ARTSENS, the neck region was palpated to identify the artery's location. The A-mode ultrasound probe was positioned around the identified region and oriented until strong echo amplitudes from the CCA artery walls were obtained. Continuous echo signals obtained from the vessel wall were recorded for thirty seconds and saved for further offline processing. Multiple measurements of thirty seconds were obtained to select the best-quality waveforms for analysis. Both the measurements were obtained in a sequential manner. Refer to supplementary Fig. 2 for study photos.

E. Data Processing

Fig. 2 illustrates an overview of the algorithm and signal processing steps involved with the data processing. The digitized ultrasound echo signals obtained from the CCA were processed to identify the vessel walls, and tracked frame to frame using previously validated algorithms [32] to obtain the diameter waveform in mm. The diameter waveform was scaled non-linearly based on the exponential pressure-diameter relationships and calibrated with brachial DBP and MAP to obtain carotid pressure waveform $P(t)$ in mmHg as in (7).

$$P(t) = \text{DBP} \times e^{\beta \left(\frac{D(t)}{D_D} - 1 \right)} \quad (7)$$

where, $D(t)$ is the diameter waveform, D_D is the end-diastolic diameter, β is the stiffness index, which is iteratively optimized, such that the mean value of $P(t)$ becomes equal to brachial MAP [33].

The Duplex mode video files with flow velocity waveforms (in cm/s) were processed using open-sourced software written in MATLAB [34]. The obtained time series waveform was calibrated with the on-screen axis to equivalent units in pixels. The measured flow waveform in ml/s was obtained as a product of flow velocity waveform with the cross-sectional area waveform of the CCA. Ten continuous cycles were used to

TABLE I
STUDY PARTICIPANTS DEMOGRAPHY

Total Participants (Male/Female)	70 (28 Female)
Age (years)	26 ± 7 (20 to 51)
Weight (kg)	66.16 ± 13.95
Height (cm)	168.70 ± 9.67
BMI (kg/m ²)	23.35 ± 4.16
Brachial Systolic BP (mmHg)	111 ± 9
Central Systolic BP (mmHg)	100 ± 9
Brachial or Central Diastolic BP (mmHg)	69 ± 7
Brachial or Central MAP (mmHg)	83 ± 7
Heart Rate (bpm)	70 ± 10

obtain a time-averaged mean pulse waveform for pressure and measured flow for WSA. Both the waveforms were time-aligned with respect to dicrotic notch of pressure waveform and ejection duration of the measured flow.

The calibrated pressure waveform and measured flow were filtered using a zero-phase Butterworth low pass filter (order: 2, cut-off frequency: 15 Hz). The study participants were classified into Type-A, Type-B and Type-C waveforms based on the augmentation index calculated from the higher derivatives of the pressure waveform [28]. Estimated time instants of early systolic peak and late systolic peak were calculated from the zero-crossing of 2nd derivative waveform, as illustrated in Fig. 1. For WSA_{REF}, the pressure waveform and measured flow were converted into their frequency domain equivalent to compute the input impedance spectrum as $P(j\omega)/Q_{REF}(j\omega)$, and Z_C was estimated as an average from 4th to 10th harmonics of the input impedance spectrum [29]. The same procedure was applied to WSA_{m-RAY}. Respective $P_F(t)$ and $P_B(t)$ from WSA_{REF} and WSA_{m-RAY} were evaluated using (5) and (6).

F. Statistical Analysis

The accuracy of the modelled flow waveform, derived $P_F(t)$, $P_B(t)$ and the error in defining the time instants of the characteristic peaks of the flow waveform were reported as the root-mean-square-error (RMSE). The group average values of reflection quantification indices were reported as their mean ± standard deviation. The agreement among the reflection quantification indices obtained from WSA_{REF} and WSA_{m-RAY} were evaluated using linear regression, Pearson's correlation, and Bland-Altman Analysis. The Pearson correlation coefficient was reported as r-value, and the level of significance (α) of 0.05 was applied to all parametric tests. A p-value < 0.05 was considered statistically significant for all the parametric tests. All statistical analyses were performed using Graph Pad Prism 9 statistical software package.

III. RESULTS

A. Participants Demography

A detailed description of the participant's demography is highlighted in Table I. The Body Mass Index (BMI) of the participants ranged from 15.6 kg/m² to 36.4 kg/m². The participants with age > 40 had higher values of BMI, higher brachial SBP and DBP, and higher central SBP and DBP ($p < 0.05$). All women

participants were premenopausal and non-pregnant. None of the participants were under any prescribed medications during the study period.

B. Reliability of the Signals

The ultrasound signal echoes from CCA obtained from the ARTSENS had a Signal-to-Noise ratio of 20 dB, with a distension tracking resolution of 10 μ m. The diameter waveform was obtained at a frame rate of 500 Hz. The mean end-diastolic diameter (D_D) was 5.53 ± 0.90 mm, and the mean distention (ΔD) was 0.56 ± 0.14 mm among the study participants.

The video files of blood flow velocity waveforms from CCA obtained using the pulsed wave Doppler were converted to time series waveforms and up sampled to 500 Hz. The flow velocity waveforms have reliably captured the early systolic and late systolic peaks of the CCA blood flow waveform. The mean peak systolic flow velocity and flow rate values were 56.76 ± 13.93 cm/s and 14.02 ± 5.60 ml/s, respectively. Refer to supplementary Fig. 3 for sample waveforms of diameter and measured flow.

C. Accuracy of the Modelled Flow Shape and Agreement in Characteristic Impedance

Fig. 3(a)–(c) compares the modelled flow with measured flow waveform. The RMSE in the morphology of modelled flow with the measured flow was 0.20 A.U. The RMSE in estimation of the amplitude ratio was 0.09 A.U, which is the error associated with the shape of late systolic flow peak. The early systolic flow peak is always scaled to 1. The RMSE in the time instants of the early systolic peak was 16.75 ms ($\sim 2\%$ of the average cardiac cycle length of the study participants), and of the late systolic peak was 26.76 ms ($\sim 3.3\%$ of the average cardiac cycle length of the study participants). In frequency domain analysis, the correspondence between the magnitude spectrum harmonics of the modelled flow and measured flow up to 15 Hz has a statistically significant and strong correlation of (mean $r = 0.95$, $p < 0.001$), highlighting the agreement between modelled and measured flow. The Z_C estimated using $Q_{m-RAY}(j\omega)$ and $Q_{REF}(j\omega)$ reveals a statistically significant strong correlation ($r = 0.90$, $p < 0.001$) as depicted in Fig. 4(a). Bland-Altman Analysis reveals insignificant bias and a dispersed plot, as shown in Fig. 4(d), highlighting no systematic progression of errors.

D. Forward-Backward Pressure Wave Separation

Fig. 3(d)–(f) illustrates $P_F(t)$ and $P_B(t)$ derived from WSA_{REF} and WSA_{m-RAY} for Type-A, Type-B and Type-C participants. The RMSE in $P_F(t)$ and $P_B(t)$ was 2.18 ± 0.97 mmHg ($\sim 2.5\%$ of the average MAP of the study participants). The group average $\Delta P_{F REF}$, and $\Delta P_{F m-RAY}$ were 25.61 ± 5.04 mmHg and 25.27 ± 5.35 mmHg, respectively. Similarly, the group average $\Delta P_{B REF}$, and $\Delta P_{B m-RAY}$ were 12.05 ± 3.16 mmHg and 12.97 ± 3.22 mmHg, respectively. Fig. 4(b)–(c) and (e)–(f) depicts the regression and Bland-Altman analysis for ΔP_F , ΔP_B obtained from WSA_{REF} and WSA_{m-RAY}. Statistically significant and strong correlations

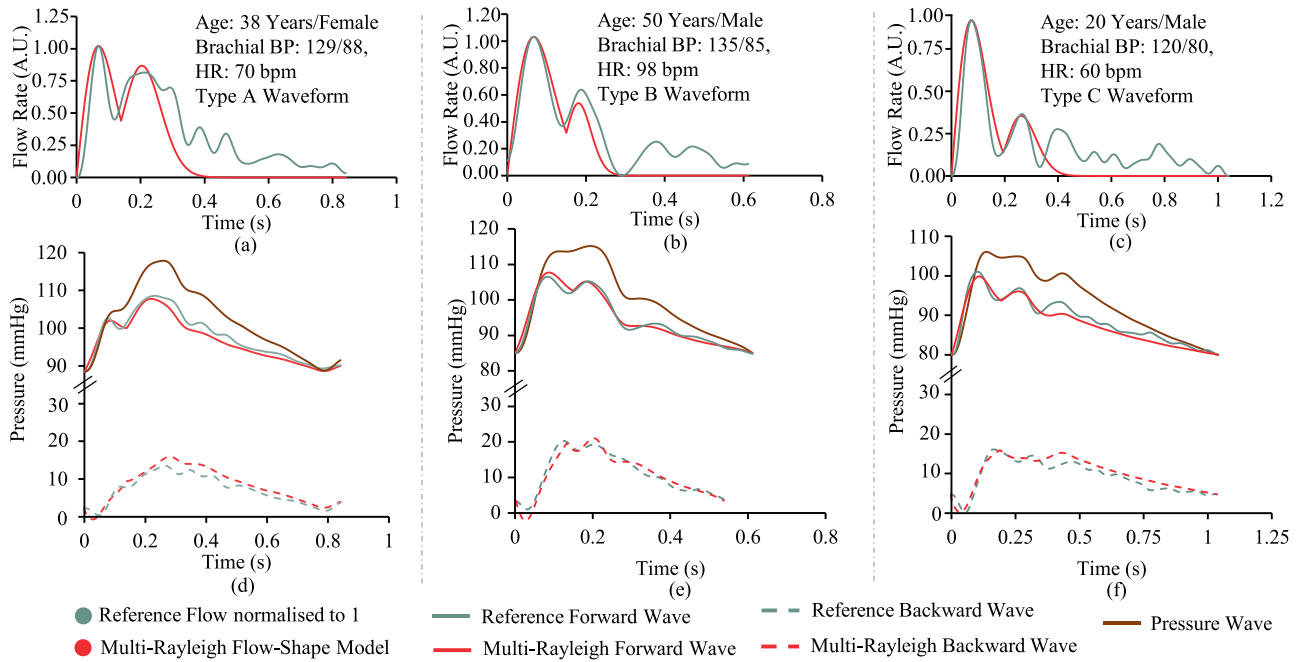


Fig. 3. Comparison of multi-rayleigh modelled flow-shape waveform with the reference waveform, both normalized to 1 (a) for a type-A waveform, (b) for a type-B waveform, (c) for a Type-C waveform. Comparison of forward and backward pressure waveform obtained from WSA_{REF} and WSA_{m-RAY} (d) for a type-A waveform, (e) for a type-B waveform, (f) for a type-C waveform.

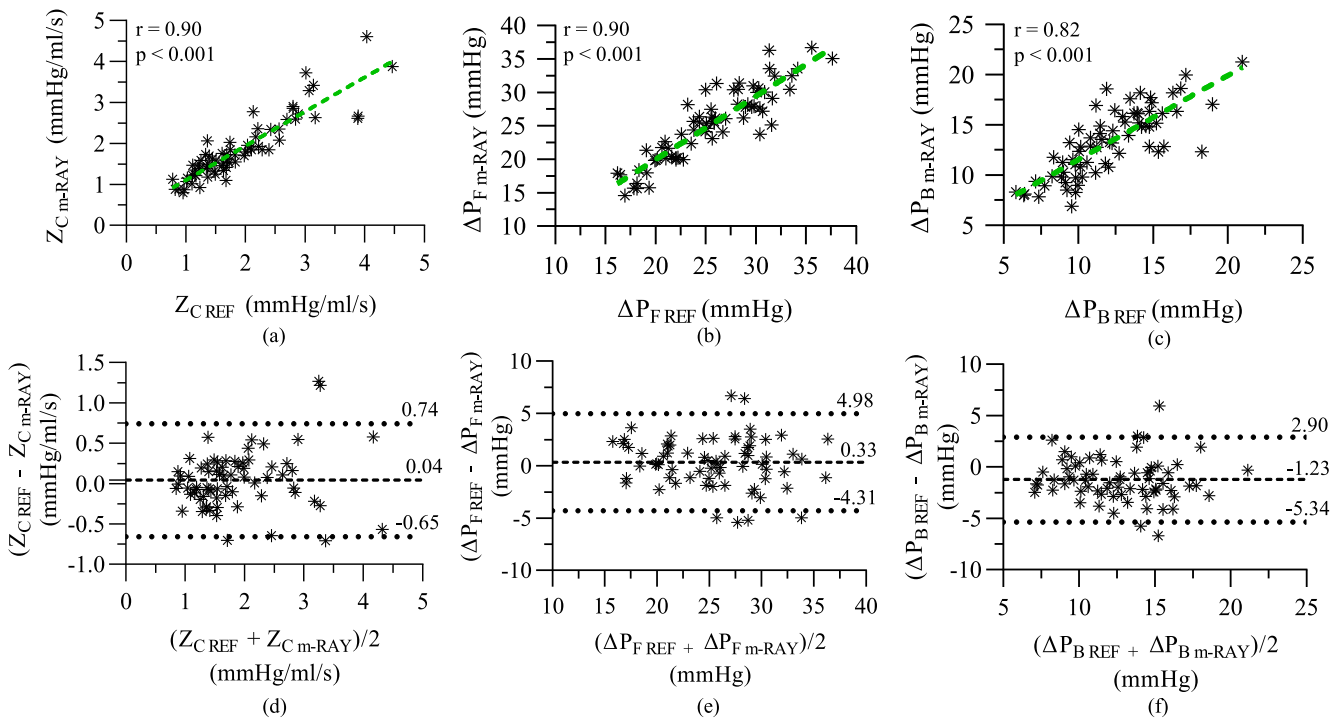


Fig. 4. (a)–(c) Regression analysis of Z_C , ΔP_F , ΔP_B obtained from WSA_{REF} and WSA_{m-RAY} with their respective Pearson correlation coefficient, (d)–(f) Bland altman analysis of Z_C , ΔP_F , ΔP_B obtained from WSA_{REF} and WSA_{m-RAY} with their respective bias and limits of agreement.

were observed between ΔP_{F_REF} , and ΔP_{F_m-RAY} ($r = 0.90$, $p < 0.001$) and between ΔP_{B_REF} , and ΔP_{B_m-RAY} ($r = 0.82$, $p < 0.001$). The bias between ΔP_{F_REF} , and ΔP_{F_m-RAY} was 0.33 ± 2.37 mmHg ($p = 0.35$), and between ΔP_{B_REF} , and ΔP_{B_m-RAY} was -0.91 ± 1.97 mmHg ($p = 0.04$).

Fig. 5(a)–(b) and (d)–(e) depicts the regression and Bland-Altman analysis for mean P_F and mean P_B obtained from WSA_{REF} and WSA_{m-RAY} . Similar to the results of pulse pressures, a statistically significant and strong correlations were observed between mean P_{F_REF} , and mean P_{F_m-RAY} ($r = 0.99$,

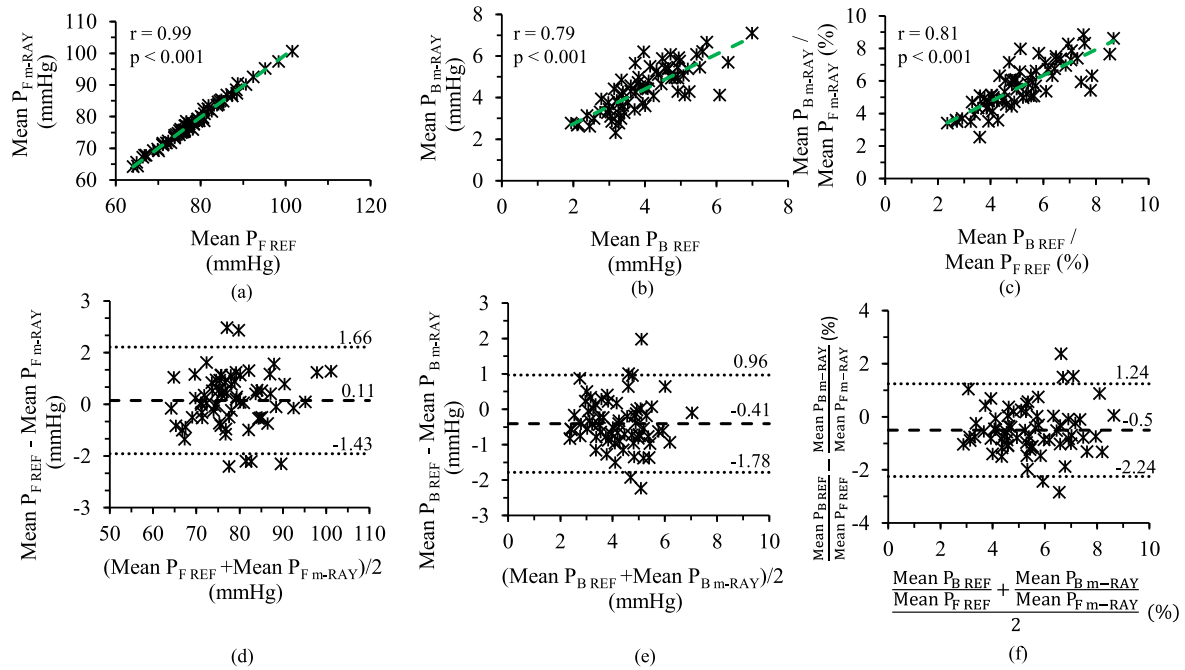


Fig. 5. (a)–(c) Regression analysis of mean P_F , mean P_B , mean $P_B/\text{mean } P_F$ obtained from WSA_{REF} and $\text{WSA}_{\text{m-RAY}}$ with their respective Pearson correlation coefficient, (d)–(f) bland altman analysis of mean P_F , mean P_B , mean $P_B/\text{mean } P_F$ obtained from WSA_{REF} and $\text{WSA}_{\text{m-RAY}}$.

$p < 0.001$) and between mean $P_{B \text{ REF}}$, and mean $P_{B \text{ m-RAY}}$ ($r = 0.79$, $p < 0.001$). The bias between mean $P_{F \text{ REF}}$, and mean $P_{F \text{ m-RAY}}$ was 0.11 ± 0.79 mmHg and between mean $P_{B \text{ REF}}$, and mean $P_{B \text{ m-RAY}}$ was $-0.41 \text{ brk} \pm 0.70$ mmHg.

E. Performance Evaluation Based on Reflection Quantification

The group average values for $\text{RM}_{\text{m-RAY}}$, $\text{RI}_{\text{m-RAY}}$ and $\text{RWTT}_{\text{m-RAY}}$ were 0.54 ± 0.14 , $34.86 \pm 5.89\%$, and 75.54 ± 11.31 ms respectively. Whereas the group average values for RM_{REF} , RI_{REF} and RWTT_{REF} were 0.50 ± 0.13 , $31.99 \pm 5.69\%$, and 67.70 ± 15.54 ms respectively. Fig. 6 depicts the regression and Bland-Altman analysis between reflection quantification indices (RM, RI and RWTT) obtained from WSA_{REF} and $\text{WSA}_{\text{m-RAY}}$. A moderately strong and statistically significant correlation between $\text{RM}_{\text{m-RAY}}$ and RM_{REF} ($r = 0.81$, $p < 0.001$), $\text{RI}_{\text{m-RAY}}$ and RI_{REF} ($r = 0.80$, $p < 0.001$), and $\text{RWTT}_{\text{m-RAY}}$ and RWTT_{REF} ($r = 0.76$, $p < 0.001$) was observed. Fig. 5(c) and (f) reveals the correlation and bland-Altman analysis for the ratio of mean P_B to mean P_F obtained from WSA_{REF} and $\text{WSA}_{\text{m-RAY}}$. Statistically significant correlation ($r = 0.81$, $p < 0.001$) with bias of -0.5% was observed. Bland-Altman analysis for all the reflection quantification indices revealed a scattered plot, indicative of no systematic progression of errors.

IV. DISCUSSION

The CCA flow waveform consists of more than one flow peak in the systolic phase, one peak in the diastolic phase, and a

non-zero flow after the ejection duration. The CCA flow is distinguishably different from the ascending aortic flow waveform. The tri-phasic nature of CCA flow is mainly attributed to the pulse wave reflections from the cerebral vasculature and reflection waves from the lower body. The early systolic flow peak is predominantly influenced by wave reflections from cerebral circulation, and the late systolic flow peak is influenced by wave reflections from the lower body [22].

Recent studies [18], [19], [20], [21], [22] have indicated a possible connection between the arterial phenotypes of the upper body and the development of cerebral microvascular diseases. The underlying vascular pathophysiology behind cerebral microvascular diseases is related to the strength of the pulse waves induced in the craniospinal cavity by the upper body vasculature [23]. Increased wave reflections from cerebral circulation increase the pulse pressure in the carotid artery and decrease the flow into the brain [4]. Therefore, it is essential to model the early and late systolic flow peaks for reliable quantification of wave reflection using WSA at CCA. Although there have been several attempts to develop simplified approaches to WSA [12], [13], [14], [15], [16], [17], all of them were limited to the aortic site alone. The distinguishable differences in the flow waveform morphology between the aorta and CCA limit the applicability of the above approaches for carotid WSA. The proposed approach enables simplified WSA using a single pulse waveform measurement such as diameter scaled pressure waveform or tonometer pulse-scaled pressure waveform from easily accessible measurement sites without the requirement of additional flow measurement.

In our approach, we derive the characteristics of the CCA flow waveform from higher derivative fiducial points of the pressure

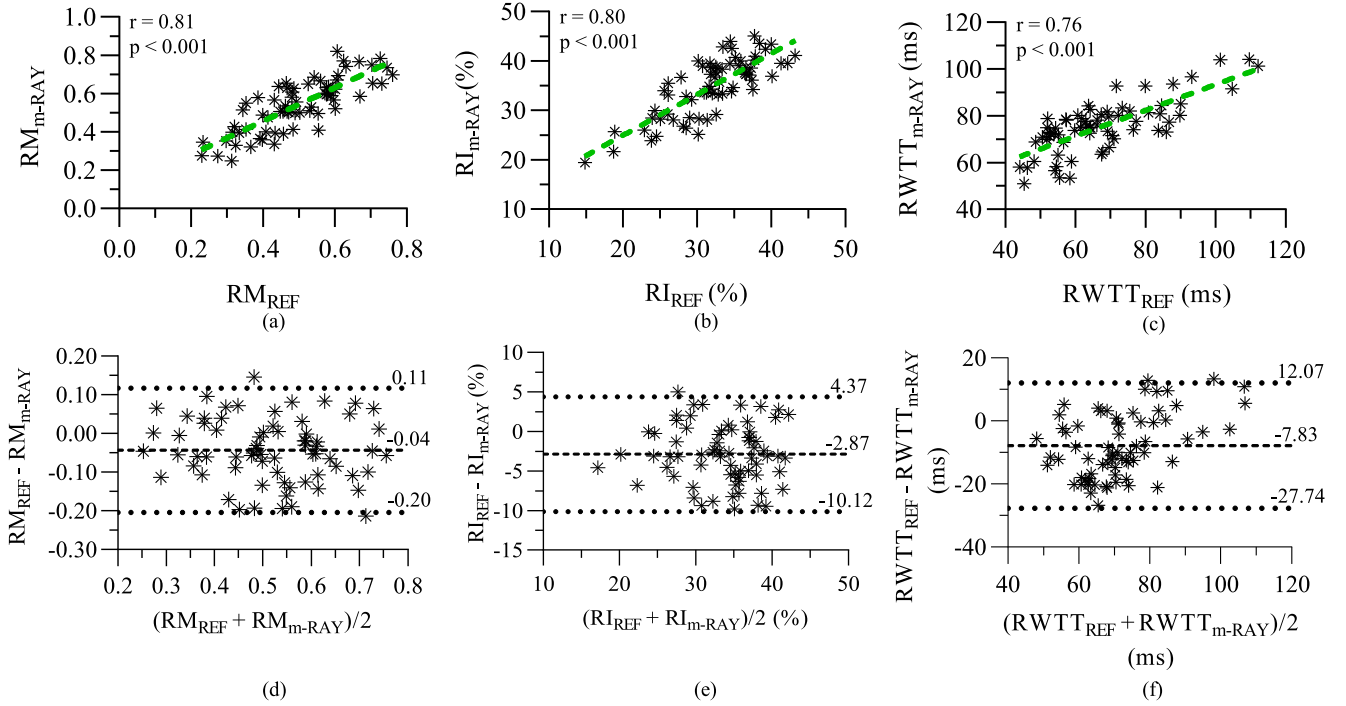


Fig. 6. (a)–(c) Regression analysis of RM, RI and RWTT obtained from WSA_{REF} and WSA_{m-RAY} with their respective pearson correlation coefficient, (d)–(f) bland altman analysis of RM, RI and RWTT obtained from WSA_{REF} and WSA_{m-RAY} with their respective bias and limits of agreement.

waveform. The pulse wave analysis is a reliable approach for the identification of fiducial points of the pressure waveform through its derivatives that have an association with the flow waveform and pulse wave reflections. The pressure and flow are coupled inherently through impedance, and any mismatch in the impedance of the arterial network would simultaneously have effects on both the wave shape of pressure and flow. This coupling between pressure and flow is advantageous for developing simplified models of flow for WSA. The amplitude ratio of the flow peaks (A_{LS}/A_{ES}) in the systolic phase of CCA flow is strongly correlated and associated with the augmentation index of the pressure waveform [22]. From our supplementary analysis (refer to supplementary Fig. 4) performed on 4374 in-silico virtual subjects [35], it was observed that the A_{LS}/A_{ES} exhibited an exponential relationship with augmentation index and with a statistically significant and strong correlation ($r = 0.70$, $p < 0.001$), consistent with the observations previously reported for 286 in-vivo study participants [22]. The pressure augmentation index is calculated from the carotid pressure waveform based on the identification of inflection or shoulder point from higher derivatives [28], [30]. Accordingly, the waveform is classified as Type-A, Type-B or Type-C. The virtual subjects dataset used to arrive at the exponential model consists of the age group 25 to 75 years, with a proportional spread of all types of waveforms. Additionally, we observed the time instants of zero-crossing of the second derivative waveform of pressure waveform, as illustrated in Fig. 1, were associated with the time instants of the flow waveform peaks. The construction of the modelled flow involves estimating the time instants of early systolic flow peak

and late systolic flow peak from the pulse contours of the pressure waveform. These estimations serve as indirect substitutes for the actual measurements. To validate these estimates derived from the 2nd derivative waveform of pressure waveform, we compared them with the actual measurements of time instants of flow peaks using on 4374 in-silico virtual subjects [35] and the results are depicted in the Supplementary Section (refer to supplementary Fig. 5). The absolute difference in mean values between the true time instant of the early systolic flow peak (0.0593 s) and estimated time instant (0.0599 s) was $< 1\%$ ($p = 0.002$). Similarly, the difference in mean values between the true time instant of the late systolic flow peak (0.194 s) and estimated time instant (0.180 s) was $< 7.5\%$ ($p < 0.001$). Given the significance of the early systolic peak in WSA, the low absolute error and overall agreement in the range of values and mean differences support using these derived estimates for flow modelling. Our approach for flow shape modelling is grounded in the underlying relationship between the pulse contours of actual carotid flow and the pressure waveform, explored as the amplitude ratio (A_{LS}/A_{ES}) and estimated time instants (t_{LS} and t_{ES}).

In WSA, the product $Z_C \times Q(t)$ becomes ratio metric, i.e., Z_C assumes an arbitrary unit, for a normalized $Q(t)$, preserving the product $Z_C \times Q(t)$. This property allows for techniques to model the flow waveform shape, which can then serve as a substitute for measured flow data in WSA and obtain forward and backward pressure waveforms. The WSA_{m-RAY} reduces the measurement complexity by modelling the flow waveform shape, targeted at scenarios with limited resources, where

comprehensive equipment and specialized personnel are often lacking, especially serves its purpose outside of a hospital setting.

In this in-vivo study, the performance of WSA_{m-RAY} was evaluated by comparing the correlation coefficient between reflection quantification indices (ΔP_F , ΔP_B , mean P_F , mean P_B , RM, RI, RWTT) derived from WSA_{REF} and WSA_{m-RAY} ($r > 0.76$, $p < 0.001$). The $P_F(t)$ and $P_B(t)$ obtained from WSA_{m-RAY} yielded a RMSE of 2.18 ± 0.97 mmHg. The simplified aortic WSA methods based on physiologic flow modelling and Windkessel flow models yielded RMSE in a similar range, whereas triangular flow modelling has reported RMSE up to 7.35 mmHg [14] for $P_F(t)$ and $P_B(t)$. The triangular approach to model the flow waveform often was observed to produce spikes in the $P_F(t)$ and $P_B(t)$ [13], [16], which was absent in the WSA performed using measured flow, averaged flow model [13], and personalized flow model [16], [17]. The WSA_{m-RAY} also did not exhibit any spikes in the $P_F(t)$ and $P_B(t)$. The values of ΔP_F and ΔP_B for an age group of 20–50 years were reported [12], [13], [14], [15], [16], [17] in the range of 21 mmHg to 35 mmHg for ΔP_F and 10 mmHg to 18 mmHg for ΔP_B among in-vivo studies and were in range to the values obtained using WSA_{m-RAY} and WSA_{REF} in the current study.

The mean values of RM, RI and RWTT observed for simplified WSA methods adopted for aortic flow were in the range of 0.63 ± 0.1 to 0.72 ± 0.07 , $38.0 \pm 4.0\%$ to $48.03 \pm 1.55\%$ and 70.0 ± 10.0 ms to 80.4 ± 15.8 ms respectively. Although not directly comparable, the values obtained in this study for both WSA_{m-RAY} and WSA_{REF} are also in similar ranges [12], [13], [14], [15], [16], [17]. The WSA_{REF} performed on carotid artery reports RM with a mean value of 0.68 ± 0.10 to 0.76 ± 0.10 and RI with a mean value of $40.0 \pm 4.0\%$ to $43.0 \pm 3.0\%$ from in-vivo study with an average age of 49 ± 17 years [36]. Whereas, in the current study, with an average age of 26 ± 7 years, the mean values of RM and RI were observed to be lower than those reported with a higher mean age. The only other simplified pressure-only WSA on CCA was our previous work using multi-Gaussian decomposition [27] of pressure waveform performed on an in-silico database, which revealed values of RM, RI, RWTT in the ranges of 0.79 ± 0.08 , $44.23 \pm 2.58\%$ and 45.50 ± 5.56 ms respectively for mean age of 45 ± 10 years. These observations were concurrent with the group average values observed in this study after accounting for the lower mean age.

As a supplementary analysis, we have compared the performance of multi-Gaussian, multi-Rayleigh and triangular-shape (WSA_{TF}) for modelling flow shape and perform WSA on the same in-vivo dataset and a comparative performance is tabulated in the supplementary section (Supplementary Tables I and II). For WSA_{TF} and WSA_{MGD} the mean values of reflection quantification indices - ΔP_F , ΔP_B , RM, RI are comparable ranges for the in-vivo study population, the RWTT has deviated by 30.3 ms and 11 ms respectively. It may be noted that the multi-Gaussian approach [27] depends on $\sim 20\%$ of the dataset with measured or reference flow waveform as a training set for designing the model parameters. Therefore, the reflection quantification may perform better on the dataset on which the

model was trained. In comparison, the proposed multi-Rayleigh approach does not depend on any dataset, is computationally less intensive (fewer parameters to optimize) and can be applied to any pulse waveforms recorded from CCA. The Rayleigh functions enable modulation of upslope and downslope steepness with just one parameter, streamlining adjustments compared to the multiple parameters needed for Gaussian and Log-normal functions. Furthermore, Rayleigh functions provide a smoother profile than triangular approximations.

The performance of WSA_{m-RAY}, (or any similar approaches) depends on the reliability of the flow shape modelling. It was observed that the modelled flow has reliably captured the relative time instants of early and late systolic flow peaks and their amplitude ratio with an RMSE of 0.09 A.U. The systolic phase accounts for nearly 95 percentile of the energy content of the flow waveform, and therefore, the proposed modelling approach was confined to the systolic phase of the flow waveform [37]. The accuracy of the modelled flow was supplemented by the agreement of Z_C ($r = 0.90$, $p < 0.001$) between the modelled and measured flow. The time domain agreement between modelled and measured flow in terms of low RMSE for waveform morphology, time instants of flow peaks and ejection duration demonstrates the accuracy of flow modelling for WSA. The RMSE for modelled flow was observed to be at par with modelling approaches used for aortic flow for in-vivo and in-silico data [12], [13], [14], [15], [16], [17]. The frequency domain agreement between modelled and measured flow was determined through the high correlation coefficient between the amplitudes of the magnitude spectrum and the strong correlation among Z_C . The multi-Gaussian approach for CCA flow modelling [27] was limited in modelling to the early systolic peak. The accuracy of multi-Rayleigh modelled Z_C (as % error in bias with respect to $Z_{C\text{ REF}}$) was observed to be improved in comparison to multi-Gaussian Z_C (2.11% vs. 4.5%) [38] for CCA.

The simplified pressure-only WSA methods, as elucidated in this article, pave the way for executing large-scale field studies in resource-constrained environments. Furthermore, to compute the reflection quantification indices, WSA can be evaluated directly from diameter waveform, without requiring to convert to pressure waveform, thus eliminating additional uncertainty due to the pressure calibration [9], [10], [11]. This evaluation is particularly pertinent for scenarios with limited resources, where comprehensive equipment and specialized personnel are often lacking. Especially such methods aid in conducting large-scale resource constrained field studies bypassing the need for a hospital setting for measurements. This can be achieved using a tonometer, single element ultrasound transducers or a photoplethysmogram sensor to acquire non-invasive pulse waveforms from the CCA, which can be scaled to pressure waveform. The ARTSENS is only an example of such use-cases, and the applicability of the proposed method – WSA_{m-RAY} is in no way limited to ARTSENS. The utility of the method can be achieved using any non-invasive instrument capable of deriving an arterial pulse waveform such as carotid tonometry, photoplethysmogram or diameter waveform from ultrasound scans.

V. LIMITATIONS AND FUTURE SCOPE

The in-vivo study was conducted on an age group limited to 51 years, and the percentage of female participants was 40%. The WSA_{m-RAY} has been validated only on a healthy population aged between 20 to 51, with no other pathologies and BMI lower than 30 kg/m^2 . The WSA_{m-RAY} depends on high-fidelity pulse waveforms to ensure accurate identification of fiducial points from higher derivative waveform. Filtering methods of pulse waveforms and derivatives may introduce temporal shifts on the fiducial points. Therefore, employing signal processing algorithms immune to such temporal shifts can significantly enhance the accuracy and precision of WSA_{m-RAY} . The amplitude ratio (A_{LS}/A_{ES}) used in this study is based on a statistical model from a healthy virtual population. Learning-based algorithms may improve this model, enabling a more comprehensive representation that encompasses both diseased and healthy populations. The WSA_{m-RAY} assumes an absence of retrograde flow in CCA as it was not prevalent in the healthy population. Further research is in progress to enhance the WSA_{m-RAY} for other peripheral arterial sites by including retrograde flow modelling. In the proposed method, we have achieved comparable accuracies and agreement for the flow waveform shape modelling and estimation of Z_C , which are critical for performing WSA. The waveform shape approximation without considering the diastolic phase becomes more relevant for peripheral arteries, where retrograde flow is also more significant. As the relationship between the amplitude ratio of systolic phase flow peaks to augmentation index of the pressure waveform was used in the modelling; Such a relationship connecting the third flow peak in diastolic phase warrants further investigation to be able to use for modeling the flow. The modelling of the third flow peak was not attempted in the current study, as comparable accuracies and strong correlation with reference method was obtained for the characteristic impedance and derived forward-backward pressure waveforms by only considering the flow modelling in the systolic phase. From a measurement's perspective, although usage of tonometry or single element ultrasound transducers warrants training of the operator to acquire better quality signals. The usage of such noninvasive technologies bypasses the hospital settings, enabling large-scale field studies for cardiovascular screening under resource constraints. Additional epidemiological trials would also explore the clinical significance of reflection quantification indices as potential prognostic markers for central and cerebral pathophysiology.

VI. CONCLUSION

The CCA flow waveform was modelled, preserving the characteristic flow peaks in the early and late systolic phases using weighted and shifted multi-Rayleigh functions. The modelled flow and pressure waveform from the CCA served as the basis for performing WSA_{m-RAY} . The accuracy of the modelled flow waveform and the performance of WSA_{m-RAY} were evaluated from an in-vivo study conducted on 70 participants (28 female, aged 20 to 51 years). The comparable accuracies in forward and backward pulse waves obtained from WSA_{REF} and WSA_{m-RAY}

prove the usability of modelled flow shape for performing WSA at the carotid artery. Furthermore, statistically significant and strong correlation ($r > 0.76$, $p < 0.001$) was observed between reflection quantification indices (ΔP_F , ΔP_B , mean P_F , mean P_B , RM, RI, RWTT) from WSA_{REF} and WSA_{m-RAY} . The proposed approach therefore enables simplified WSA using a single pulse waveform measurement from easily accessible arterial measurement sites without the requirement of additional flow measurement. The WSA_{m-RAY} has the potential to expand the scope of clinical investigations, offering valuable insights into both central and cerebral pathophysiology. The usage of such noninvasive technologies bypasses the need for a hospital setting, enabling large-scale field studies for cardiovascular screening.

REFERENCES

- [1] A. Diaz et al., "Non-invasive central aortic pressure measurement: What limits its application in clinical practice?," *Front. Cardiovasc. Med.*, vol. 10, no. 5, pp. 1–5, 2023, doi: [10.3389/fcvm.2023.1159433](https://doi.org/10.3389/fcvm.2023.1159433).
- [2] M. M. Pereira et al., "Wave separation analysis-derived indexes obtained from radial and carotid tonometry in healthy pregnancy and pregnancy-associated hypertension: Comparison with pulse wave analysis-derived indexes," *Front. Cardiovasc. Med.*, vol. 9, no. 9, pp. 1–13, 2022, doi: [10.3389/fcvm.2022.997452](https://doi.org/10.3389/fcvm.2022.997452).
- [3] D. Terentes-Printzios, V. Gardikioti, and C. Vlachopoulos, "Central over peripheral blood pressure: An emerging issue in hypertension research," *Heart, Lung Circulation*, vol. 30, no. 11, pp. 1667–1674, Nov. 2021, doi: [10.1016/j.hlc.2021.07.019](https://doi.org/10.1016/j.hlc.2021.07.019).
- [4] J. P. Mynard and A. Kondiboyina, "Wave reflection in the arterial tree," in *Textbook of Arterial Stiffness and Pulsatile Hemodynamics in Health and Disease*, J. A. Chirinos, Ed., Cambridge, MA, USA: Academic, 2022, pp. 169–194, doi: [10.1016/B978-0-323-91391-1.00011-X](https://doi.org/10.1016/B978-0-323-91391-1.00011-X).
- [5] J. Hashimoto et al., "Different role of wave reflection magnitude and timing on left ventricular mass reduction during antihypertensive treatment," *J. Hypertens.*, vol. 26, no. 5, pp. 1017–1024, 2008, doi: [10.1097/HJH.0b013e3282f62a9b](https://doi.org/10.1097/HJH.0b013e3282f62a9b).
- [6] M. A. Haidar et al., "Wave reflection at the origin of a first-generation branch artery and target organ protection: The AGES-Reykjavik study," *Hypertension*, vol. 77, no. 4, pp. 1169–1177, 2021, doi: [10.1161/HYPERTENSIONAHA.120.16696](https://doi.org/10.1161/HYPERTENSIONAHA.120.16696).
- [7] N. Westerhof et al., "Forward and backward waves in the arterial system," *Cardiovasc. Res.*, vol. 6, no. 6, pp. 648–656, 1972, doi: [10.1093/cvr/6.6.648](https://doi.org/10.1093/cvr/6.6.648).
- [8] K. H. Parker, "An introduction to wave intensity analysis," *Med. Biol. Eng. Comput.*, vol. 47, no. 2, pp. 175–188, 2009, doi: [10.1007/s11517-009-0439-y](https://doi.org/10.1007/s11517-009-0439-y).
- [9] J. Feng and A. W. Khir, "Determination of wave speed and wave separation in the arteries using diameter and velocity," *J. Biomech.*, vol. 43, no. 3, pp. 455–462, 2010, doi: [10.1016/j.jbiomech.2009.09.046](https://doi.org/10.1016/j.jbiomech.2009.09.046).
- [10] N. Pomella et al., "Common carotid artery diameter, blood flow velocity and wave intensity responses at rest and during exercise in young healthy humans: A reproducibility study," *Ultrasound Med. Biol.*, vol. 43, no. 5, pp. 943–957, May 2017, doi: [10.1016/j.ultrasmedbio.2016.12.018](https://doi.org/10.1016/j.ultrasmedbio.2016.12.018).
- [11] N. Pomella et al., "Noninvasive assessment of the common carotid artery hemodynamics with increasing exercise work rate using wave intensity analysis," *Amer. J. Physiol.-Heart Circulatory Physiol.*, vol. 315, no. 2, pp. H233–H241, 2018, doi: [10.1152/ajpheart.00667.2017](https://doi.org/10.1152/ajpheart.00667.2017).
- [12] B. E. Westerhof et al., "Quantification of wave reflection in the human aorta from pressure alone: A proof of principle," *Hypertension*, vol. 48, no. 4, pp. 595–601, 2006, doi: [10.1161/01.HYP.0000238330.08894.17](https://doi.org/10.1161/01.HYP.0000238330.08894.17).
- [13] J. G. Kips et al., "Evaluation of noninvasive methods to assess wave reflection and pulse transit time from the pressure waveform alone," *Hypertension*, vol. 53, no. 2, pp. 142–149, 2009, doi: [10.1161/HYPERTENSIONAHA.108.123109](https://doi.org/10.1161/HYPERTENSIONAHA.108.123109).
- [14] B. Hametner et al., "Wave reflection quantification based on pressure waveforms alone-methods, comparison, and clinical covariates," *Comput. Methods Programs Biomed.*, vol. 109, no. 3, pp. 250–259, 2013, doi: [10.1016/j.cmpb.2012.10.005](https://doi.org/10.1016/j.cmpb.2012.10.005).

- [15] L. Hao et al., "Feasibility of waveform separation of central aortic pressure pulse based on lognormal flow wave approximation," *Biomed. Signal Process. Control*, vol. 77, Aug. 2022, Art. no. 103784, doi: [10.1016/j.bspc.2022.103784](https://doi.org/10.1016/j.bspc.2022.103784).
- [16] H. Sun et al., "Wave reflection quantification analysis and personalized flow wave estimation based on the central aortic pressure waveform," *Front. Physiol.*, vol. 14, no. 2, pp. 1–17, 2023, doi: [10.3389/fphys.2023.1097879](https://doi.org/10.3389/fphys.2023.1097879).
- [17] N. Shenouda et al., "Personalized physiologic flow waveforms improve wave reflection estimates compared to triangular flow waveforms in adults," *Amer. J. Physiol.-Heart Circulatory Physiol.*, vol. 320, no. 5, pp. H1802–H1812, 2021, doi: [10.1152/ajpheart.00747.2020](https://doi.org/10.1152/ajpheart.00747.2020).
- [18] E. C. Schroeder et al., "Acute systemic inflammation reduces both carotid and aortic wave reflection in healthy adults," *Physiol. Rep.*, vol. 7, no. 15, 2019, Art. no. e14203, doi: [10.14814/phy2.14203](https://doi.org/10.14814/phy2.14203).
- [19] W. K. Lefferts, J. A. Augustine, and K. S. Heffernan, "Effect of acute resistance exercise on carotid artery stiffness and cerebral blood flow pulsatility," *Front. Physiol.*, vol. 5, no. 3, pp. 1–10, 2014, doi: [10.3389/fphys.2014.00101](https://doi.org/10.3389/fphys.2014.00101).
- [20] N. Ohte et al., "Clinical usefulness of carotid arterial wave intensity in assessing left ventricular systolic and early diastolic performance," *Heart Vessels*, vol. 18, no. 3, pp. 107–111, 2003, doi: [10.1007/s00380-003-0700-5](https://doi.org/10.1007/s00380-003-0700-5).
- [21] K. Hirata et al., "Age-related changes in carotid artery flow and pressure pulses: Possible implications for cerebral microvascular disease," *Stroke*, vol. 37, no. 10, pp. 2552–2556, 2006, doi: [10.1161/01.STR.0000242289.20381.f4](https://doi.org/10.1161/01.STR.0000242289.20381.f4).
- [22] J. Hashimoto, B. E. Westerhof, and S. Ito, "Carotid flow augmentation, arterial aging, and cerebral white matter hyperintensities: Comparison with pressure augmentation," *Arteriosclerosis, Thromb., Vasc. Biol.*, vol. 38, no. 12, pp. 2843–2853, 2018, doi: [10.1161/ATVBAHA.118.311873](https://doi.org/10.1161/ATVBAHA.118.311873).
- [23] G. A. Bateman, "Pulse wave encephalopathy: A spectrum hypothesis incorporating alzheimer's disease, vascular dementia and normal pressure hydrocephalus," *Med. Hypotheses*, vol. 62, no. 2, pp. 182–187, Feb. 2004, doi: [10.1016/S0306-9877\(03\)00330-X](https://doi.org/10.1016/S0306-9877(03)00330-X).
- [24] S. T. Chiesa et al., "Carotid artery wave intensity in mid-to late-life predicts cognitive decline: The whitehall II study," *Eur. Heart J.*, vol. 40, no. 28, pp. 2300–2309, 2019, doi: [10.1093/eurheartj/ehz189](https://doi.org/10.1093/eurheartj/ehz189).
- [25] C. Kolyva and A. W. Khir, "Wave intensity analysis in the ventricles, carotid and coronary arteries – What has been learnt during the last 25 years?: Part 2," *Int. Cardiovasc. Forum J.*, vol. 1, no. 3, pp. 122–127, 2014. [Online]. Available: <https://icfjournal.org/index.php/icfj/article/view/36/794>
- [26] A. Zambanini et al., "Wave-energy patterns in carotid, brachial, and radial arteries: A noninvasive approach using wave-intensity analysis," *Amer. J. Physiol.-Heart Circulatory Physiol.*, vol. 289, no. 1, pp. 270–276, Jul. 2005, doi: [10.1152/ajpheart.00636.2003](https://doi.org/10.1152/ajpheart.00636.2003).
- [27] R. Manoj et al., "Arterial pressure pulse wave separation analysis using a multi-Gaussian decomposition model," *Physiol. Meas.*, vol. 43, no. 5, May 2022, Art. no. 055005, doi: [10.1088/1361-6579/ac6e56](https://doi.org/10.1088/1361-6579/ac6e56).
- [28] J. P. Murgo et al., "Aortic input impedance in normal man: Relationship to pressure wave forms," *Circulation*, vol. 62, no. 1, pp. 105–116, 1980, doi: [10.1161/01.CIR.62.1.105](https://doi.org/10.1161/01.CIR.62.1.105).
- [29] A. Swillens and P. Segers, "Assessment of arterial pressure wave reflection: Methodological considerations," *Artery Res.*, vol. 2, no. 4, pp. 122–131, 2008, doi: [10.1016/j.artres.2008.05.001](https://doi.org/10.1016/j.artres.2008.05.001).
- [30] P. Segers et al., "Assessment of pressure wave reflection: Getting the timing right!," *Physiol. Meas.*, vol. 28, no. 9, pp. 1045–1056, 2007, doi: [10.1088/0967-3334/28/9/006](https://doi.org/10.1088/0967-3334/28/9/006).
- [31] P. M. Nabeel, K. V. Raj, and J. Joseph, "Image-free ultrasound for local and regional vascular stiffness assessment: The ARTSENS plus," *J. Hypertension*, vol. 40, no. 8, pp. 1537–1544, 2022, doi: [10.1097/HJH.0000000000003181](https://doi.org/10.1097/HJH.0000000000003181).
- [32] J. Joseph et al., "Assessment of carotid arterial stiffness in community settings with ARTSENS," *IEEE J. Transl. Eng. Health Med.*, vol. 9, 2021, Art. no. 1900111, doi: [10.1109/JTEHM.2020.3042386](https://doi.org/10.1109/JTEHM.2020.3042386).
- [33] J. M. Meinders and A. P. G. Hoeks, "Simultaneous assessment of diameter and pressure waveforms in the carotid artery," *Ultrasound Med. Biol.*, vol. 30, no. 2, pp. 147–154, 2004, doi: [10.1016/j.ultrasmedbio.2003.10.014](https://doi.org/10.1016/j.ultrasmedbio.2003.10.014).
- [34] C. L. Coolbaugh et al., "FloWave.US: Validated, open-source, and flexible software for ultrasound blood flow analysis," *J. Appl. Physiol.*, vol. 121, no. 4, pp. 849–857, 2016, doi: [10.1152/japplphysiol.00819.2015](https://doi.org/10.1152/japplphysiol.00819.2015).
- [35] P. H. Charlton et al., "Modeling arterial pulse waves in healthy aging: A database for in silico evaluation of hemodynamics and pulse wave indexes," *Amer. J. Physiol.-Heart Circulatory Physiol.*, vol. 317, no. 5, pp. H1062–H1085, 2019, doi: [10.1152/AJPHEART.00218.2019](https://doi.org/10.1152/AJPHEART.00218.2019).
- [36] N. Di Lascio et al., "Effects of carotid pressure waveforms on the results of wave separation, wave intensity and reservoir pressure analysis," *Physiol. Meas.*, vol. 39, no. 11, 2018, Art. no. 114003, doi: [10.1088/1361-6579/aae6eb](https://doi.org/10.1088/1361-6579/aae6eb).
- [37] D. W. Holdsworth et al., "Characterization of common carotid artery blood-flow waveforms in normal human subjects," *Physiol. Meas.*, vol. 20, no. 3, pp. 219–240, 1999, doi: [10.1088/0967-3334/20/3/301](https://doi.org/10.1088/0967-3334/20/3/301).
- [38] R. Manoj et al., "Estimation of characteristic impedance using multi-gaussian modelled flow velocity waveform: A virtual subjects study," in *Proc. 44th Annu. Int. Conf. IEEE Eng. Med. Biol. Soc.*, 2022, pp. 2274–2277, doi: [10.1109/EMBC48229.2022.9871684](https://doi.org/10.1109/EMBC48229.2022.9871684).